12. Langevin Modeling of Intracellular Calcium Dynamics

J.W Shuai and P. Jung

Department of Physics and Astronomy and Institute for Quantitative Biology, Ohio University, Athens, OH 45701, USA

Abstract. Recent progress in fluorescent imaging technology has revealed that Ca^{2+} is released from the endoplasmic reticulum (ER) through clusters that are about 0.1μm in extent and comprise no more than 20-50 release channels. The calcium flux released by such small channel clusters exhibits significant stochasticity due to thermal fluctuations. These fluctuations have been simulated successfully by using Markov models for the binding and unbinding processes at the subunits based on the DeYoung-Keizer model (DeYoung and Keizer 1992).

For whole cell and intercellular modeling of Ca^{2+} signaling the DeYoung-Keizer model with its numerous variables is computationally too demanding. Hence, computationally less expensive but yet accurate algorithms are desirable. In this chapter we report on recent work of our group towards a Langevin approach for calcium dynamics. The starting point is the stochastic DeYoung-Keizer model. In a first step, we simplify towards a stochastic Li-Rinzel approach where the slow inactivation process is treated stochastically by a Markov process, but the other faster processes are approximated by their mean values. In a second step, the Markov process is described by a master equation that is then approximated by a Fokker-Planck equation and subsequently by a Langevin equation. The Langevin equation has the same form as the deterministic 2-variable Li-Rinzel model except that a noise-term is added where the *strength* is related to the *size of the release cluster*. We compare characteristic quantities of the calcium release such as mean values and variances, puff amplitude distributions, puff-width distributions and inter-puff interval distributions generated by an isolated cluster of release channels with all three methods and discuss conditions under which the stochastic Li-Rinzel model and the Langevin approach produce results consistent with the DeYoung-Keizer model. The Langevin approach produces results consistent with the other methods although the necessary compute time is reduced by more than a factor of 10 even for cluster sizes of 20 channels. Furthermore, the compute time required by the Langevin approach to mimic a single cluster does not increase with the size of the cluster.

12.1. Introduction

Recently, high-resolution recordings have shed new light on the elementary intracellular Ca^{2+} release events. It has been observed that the Ca^{2+} release channels are spatially organized in clusters with only 20-50 release channels and a size of about 100nm. The calcium release through such small clusters is subject to

Martin Falcke and Dieter Malchow (Eds.): LNP 623, pp. 231-252, 2003

random fluctuations due to thermal open-closed transitions of individual release channels. After Ca^{2+} is released, it rapidly diffuses within the cluster (in a few μs) and into the cytosol. There, Ca^{2+} is being absorbed by buffers and pumped back into the ER and into the extracellular space resulting in a spatially and temporally limited event that is called calcium puff or spark (Cheng et al. 1993; Callamaras et al., 1998; Melamed-Book et al. 1999; Gonzalez et al. 2000; Mak et al. 2001). Ca^{2+} blips arising from the opening of single release channels have been observed as well (Bootman et al. 1997; Lipp and Niggli 1998; Sun et al. 1998). Binding of Inositol Trisphosphate (IP_3) activates the calcium release channels and additional binding of Ca^{2+} opens the channels via Ca^{2+} induced Ca^{2+} release (Bezprozvanny et al. 1991). Puffs remain spatially restricted at low concentration of IP_3 stimulus, whereas at high levels of IP_3, neighboring clusters become functionally coupled by Ca^{2+} diffusion and Ca^{2+}-induced Ca^{2+} release so as to support intracellular Ca^{2+} waves that propagate in a saltatory manner throughout the cell. Therefore, Ca^{2+} puffs serve as elementary building blocks of intracellular Ca^{2+} waves. Moreover, puffs can arise spontaneously before a wave is initiated and can act as the triggers to initiate waves (Bootman et al., 1997). Calcium puffs provide a unique window on the dynamics of local calcium release.

In this chapter we report on recent work on stochastic modeling of the Ca^{2+} release through small clusters of release channels (IP_3Rs). In Sect. 2 we review various stochastic models that have been applied recently to account for the fluctuations in small release clusters. These include the stochastic DeYoung-Keizer model, the stochastic Li-Rinzel model and a recently applied Langevin method. In Sect. 3 we discuss results obtained for the Ca^{2+} release of isolated clusters and compare predictions of all three methods. Predictions include, puff amplitude distributions, puff lifetime distributions, inter-puff interval distributions and the approach to the deterministic limit of large channel numbers.

12.2. Stochastic Models for Ca^{2+} Release from ER

12.2.1 The Stochastic DeYoung-Keizer Model

The first theoretical model for agonist-induced Ca^{2+} oscillations based on the microscopic kinetics of IP_3 and Ca^{2+} gating of the IP_3R was proposed by DeYoung and Keizer (1992). The model assumes that three equivalent and independent subunits are involved in conduction of an IP_3R. Each subunit has one binding site for IP_3 (site 1) and two binding sites for Ca^{2+}; one Ca^{2+}-binding site (site 2) for activation, the other (site 3) for inhibition. The subunit is conducting only when site 1 and site 2 are bound and site 3 is unbound. Thus, each subunit may exist in eight states with transitions governed by second-order and first-order rate constants. The reaction scheme shown in Fig. 1 (DeYoung and Keizer 1992) illustrates the processes at a single subunit:

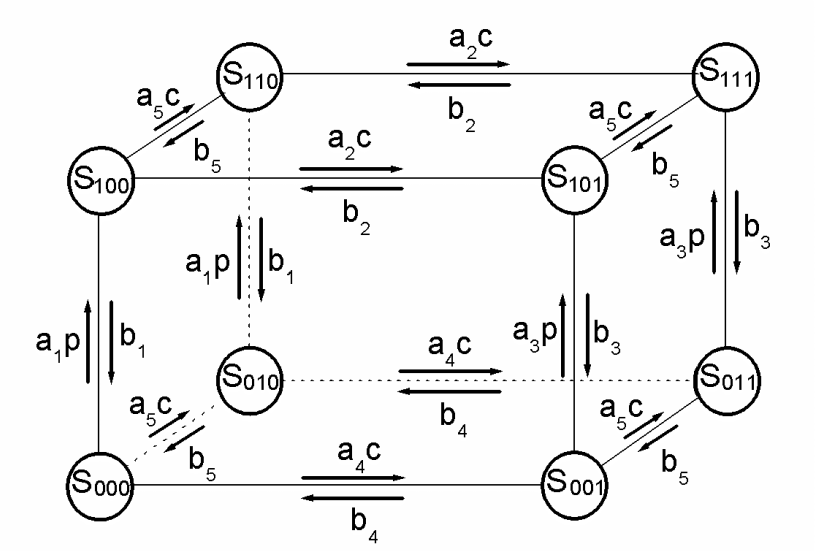

Fig. 1. The binding scheme of a single unit of the IP_3 receptor. S_{nml} denotes the probability for the subunit to be in one of the states [nml] where n,m,l can assume the values 0 and 1. The first index indicates the state of the IP_3 binding site, the second the state of the activating Ca^{2+} binding site and the third index the state of the inhibiting Ca^{2+} binding site. If an index is 0 the respective binding site is unbound; if it is 1 the respective binding site is bound. The values for the rate constants a_s and b_s are the original values used in (DeYoung and Keizer, 1992). The concentration of IP_3 is denoted by p and the intracellular concentration of Ca^{2+} is denoted by c.

For the rate constants the same rates as in (DeYoung and Keizer, 1992) are used, see the table below.

Table 1. Parameter values for the DeYoung-Keizer model of the IP_3 receptor. For the meaning of the rate constants, see **Fig. 1.**

$a_1 = 400/(\mu M\ s)$	$b_1 = 52/s$
$a_2 = 0.2/(\mu M\ s)$	$b_2 = 0.21/s$
$a_3 = 400/(\mu M\ s)$	$b_3 = 377.2/s$
$a_4 = 0.2/(\mu M\ s)$	$b_4 = 0.029/s$
$a_5 = 20/(\mu M\ s)$	$b_5 = 1.64/s$

From each state S_{ijk} the subunit can switch into three other states, as can be seen in Fig.1. Given a large ensemble of subunits, rate equations can be written for the fractions x_{ijk} of subunits being in state S_{ijk}. For the state S_{100}, for example, the following rate equation can be found

$$\begin{aligned}\frac{dx_{100}}{dt} &= pa_1x_{000} - b_1x_{100} \\ &+b_2x_{101} - a_2cx_{100} \\ &+b_5x_{110} - a_5cx_{100}\end{aligned} \quad . \tag{1}$$

Similar equations can be derived for all the other states. The fraction of open IP_3-receptors, x_{110}^3, together with leakage, determines the Ca^{2+} flux density from the ER into the intracellular space, i.e.

$$\frac{dc}{dt} = \underbrace{v_1c_1x_{110}^3(c_{ER}-c)}_{\text{channel flux}} + \underbrace{v_2c_1(c_{ER}-c)}_{\text{leakage}} - \underbrace{\frac{v_3c^2}{c^2+k_3^2}}_{\text{pump}} \tag{2}$$

with

v_1	6/s
v_2	0.11/s
v_3	0.9/(μM s)
k_3	0.1μM

and c_1=0.185. The first term denotes the flux density through the receptor channels driven by the gradient of the Ca^{2+} concentration between the ER (c_{ER}) and intracellular space (c). The second term describes a leakage flux density from the ER into the intracellular space and the third term describes the ATP driven calcium pump that removes Ca^{2+} from the intracellular space. Equation 2 and the set of kinetic equations for the x_{ijk} constitute the DeYoung-Keizer model.

Kinetic equations of the type in (1) are suitable when the numbers of channels are large and thus the fractions of channels occupying the states continuous variables. When the number of channels *N* is small, the possible fractions become discrete variables and fluctuations of the numbers of subunits in the states S_{ijk} around their expectation values become large; the standard deviation over mean value is of the order $1/\sqrt{N}$). Under these circumstances, stochastic methods have to be employed to describe the receptor dynamics.

The stochastic models for the IP_3 receptor are based on two main assumptions:

1. The transitions of the receptor states with time can be described by Markov processes

2. The underlying stochastic processes are stationary

The first assumption implies that the transition probabilities *P* of hopping within Δt to any of the three possible states "lmn" when being in state "ijk" at time *t* (see Fig.1) are only determined by the state of the system at time *t* and not by the pre-history, i.e.

$$P = P(ijk,t \mid lmn,t+\Delta t) \tag{3}$$

for all Δt. The second assumption implies that the transition probabilities are symmetric with respect to continuous time translation. Thus by subtracting t from the arguments in (3), one finds that the transition probabilities can only depend on the time difference Δt, i.e.

$$P(ijk,t \mid lmn,t+\Delta t) = P(ijk \mid lmn,\Delta t)\,. \tag{4}$$

Expanding the transition probabilities for small time steps Δt, and only retaining terms of linear order, one finds for the transition probabilities

$$P(ijk \mid lmn,\Delta t) = \Delta t \cdot r_{ijk \to lmn} \tag{5}$$

for transitions into a *different* state where the rates $r_{ijk \to klm}$ are the time derivative of the transition probabilities, and

$$P(ijk \mid ijk,\Delta t) = 1 - \Delta t \sum_{lmn \neq ijk} r_{ijk \to lmn} \tag{6}$$

for the probability remaining in the same state. In the simplest implementation of this scheme, transitions of individual subunits between states can be determined by drawing random numbers from a uniform distribution on the unit interval. Each transition represents a subinterval on the unit-interval [0,1] proportional to the value of its transition probability where the sum of all subintervals representing possible transitions (including the transition into the identical state). The transition that corresponds to the subinterval into which the random number falls is actually performed. Since we use the stochastic DeYoung-Keizer model only to produce reference values for comparison with results from approximate schemes, we do not further elaborate on more efficient simulations schemes. An example of such a simulation for a cluster of 20 IP_3Rs is shown in Fig.2.

12.2.2 The Stochastic Li-Rinzel Model

As can be seen in Fig.2, the transition rates between the states of an IP_3 channel differ significantly in their size for a large range of intracellular Ca^{2+} concentrations. The binding and unbinding of IP_3 is the fastest process, followed by the binding of Ca^{2+} the activation binding-site (approximately a factor of 10 slower) and by the binding of Ca^{2+} to the inactivation binding-site (another factor of 10 slower). Using a type of multiple time-scale expansion, Li and Rinzel (1994) were able to separate the kinetic equations for the IP_3 channel in a fast set, an intermediate set and a slow set of equations. The fast and intermediate sets of equations are solved explicitly, thus eliminating all but the slowest variables. As a result they obtain the following set of differential equations on the slowest time scale with two variables only:

$$\frac{dc}{dt} = -c_1 m_\infty^3 n_\infty^3 h^3 (c - c_{ER}) - c_1 v_2 (c - c_{ER}) - \frac{v_3 c^2}{k_3^2 + c^2} \quad (8)$$

$$\frac{dh}{dt} = \frac{1}{\tau_h}(h_\infty - h) \quad (9)$$

where the first term on the right hand side of (8) denotes the channel flux density from the ER into the intracellular space, the second term the leak flux density and the third term the pump flux density from the intracellular space into the ER. Equation (9) for h, defined as the sum of the fractions of the subunits in de-inhibited states, i.e. $h=x_{000}+x_{100}+x_{010}+x_{110}$, has the form of a two-state gate. The power h^3 in (8) indicates all three independent subunits have to be de-inhibited in order for the channel to be open. The expressions m_∞^3 and n_∞^3 describe the average fraction of the channels with bound IP_3 and bound activating Ca^{2+}, respectively. The values of the parameters above are

$$\begin{aligned} n_\infty &= \frac{p}{p+d_1} \quad ; \quad m_\infty = \frac{c}{c+d_5} \quad ; \quad \tau_h = \frac{1}{a_2(Q_2+c)} \\ h_\infty &= \frac{Q_2}{Q_2+c} \quad ; \quad Q_2 = d_2 \frac{p+d_1}{p+d_3} \quad ; \quad d_i = \frac{b_i}{a_i}. \end{aligned} \quad (10)$$

The set of equations (8,9) resemble the form of Hodgkin-Huxley neurons with only sodium channels, where the faster m activation gate-variables are replaced by their steady state value and only the slow in-activation gate is being considered dynamically. The channel current is driven by a calcium gradient instead of a voltage gradient.

The dynamic properties of the Li-Rinzel model in comparison with the DeYoung –Keizer model can be summarized in the bifurcation diagram in Fig.3. At concentrations of IP_3 of less than 0.345μM and larger than 0.644μM, the Li-Rinzel model predicts fixed points, i.e. the Ca^{2+} concentration approaches a constant value after an initial transient. A super-critical Hopf-bifurcation generates Ca^{2+} oscillations for $0.345\mu M < [IP_3] < 0.644\mu M$. The curves in the regime $0.345\mu M < [IP_3] < 0.644\mu M$ represent the minima and the maxima of $[Ca^{2+}]$ during the oscillations. The Li-Rinzel model (solid line) reproduces the bifurcation diagram of the DeYoung-Keizer model well. The upper Hopf-bifurcation, however, is somewhat shifted. The fixed-points for $[IP_3] > 0.644\mu M$ and $[IP_3] < 0.345\mu M$ are reproduced almost exactly.

We consider a cluster of N IP_3Rs, where N can be a small number and thus a stochastic description is necessary. A stochastic version of the Li-Rinzel equations can be obtained by replacing h^3 by the fraction of de-inhibited channels $N_{h-\text{open}}/N$ where N is the total number of IP_3Rs and $N_{h-\text{open}}$ is the number of channels that are de-inhibited, i.e.

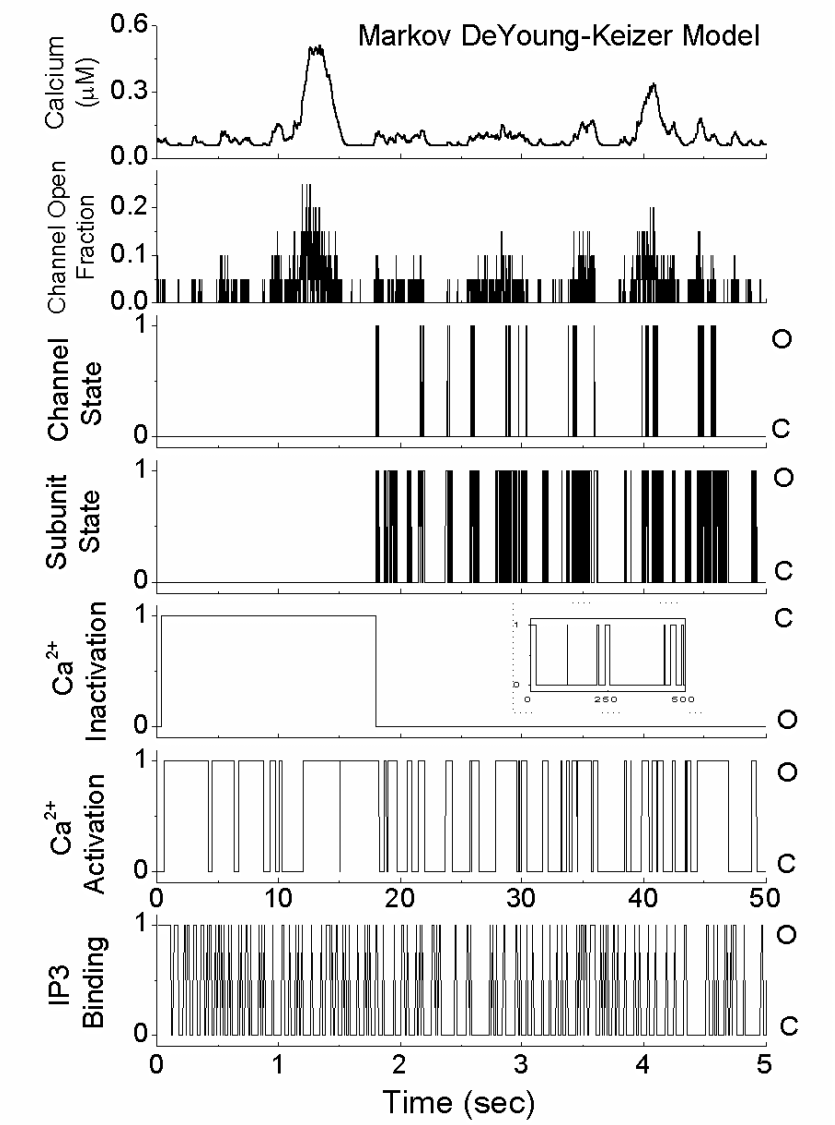

Fig. 2. The time traces of a single IP_3R embedded in a cluster of 20 IP_3Rs at [IP3]=0.3μM, simulated with the stochastic DeYoung-Keizer model are shown. The fastest process is clearly the IP_3 binding and unbinding process (lowest panel). Slower processes are calcium activation and de-activation and the slowest process is calcium inactivation (fifth panel from top). The state of one single subunit is shown in the fourth panel and the single channel state is shown in the third panel. The fraction of open channels is displayed in the second panel. The top panel displays the Ca^{2+} trace released by the cluster.

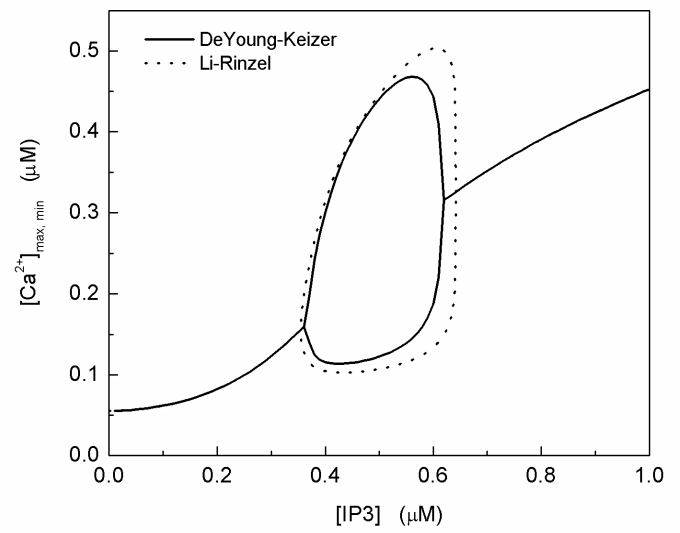

Fig. 3. Bifurcation diagram of the deterministic Li-Rinzel model (dotted line) and the DeYoung-Keizer model (solid line). Oscillations are possible between the two Hopf-bifurcations, i.e. 0.345μM<[IP_3]<0.644μM in the Li-Rinzel model. The two curves between the Hopf-bifurcations represent the minima and the maxima of [Ca^{2+}] during their oscillations. For all other values of [IP_3] fixed points are observed.

$$\frac{dc}{dt} = -c_1 m_\infty^3 n_\infty^3 \frac{N_{h-\text{open}}}{N}(c - c_{ER}) - c_1 v_2 (c - c_{ER}) - \frac{v_3 c^2}{k_3^2 + c^2} \tag{11}$$

The opening and closing rates α(p) and β(p), respectively, of this "*h*-gate" can be obtained from (10) as

$$\alpha(p) = a_2 Q_2(p) \quad ; \quad \beta(c) = a_2 c\,. \tag{12}$$

The kinetic scheme for the 4 states of the three *h*-gates of the Li-Rinzel model is given in Fig.4.

Assuming stationary Markov processes, the transition probabilities in linear order of Δt are given by the matrix (see (5))

$$S_0 \underset{\beta}{\overset{3\alpha}{\rightleftharpoons}} S_1 \underset{2\beta}{\overset{2\alpha}{\rightleftharpoons}} S_2 \underset{3\beta}{\overset{\alpha}{\rightleftharpoons}} S_3$$

Fig. 4. The kinetic scheme of the *h*-gates of the Li-Rizel model. The symbol S_n denots an IP_3R with *n h*-gates open (not inhibited). The channel is open in the state S_3.

$$\begin{pmatrix} P(0\mid 0,\Delta t) & P(0\mid 1,\Delta t) & P(0\mid 2,\Delta t) & P(0\mid 3,\Delta t) \\ P(1\mid 0,\Delta t) & P(1\mid 1,\Delta t) & P(1\mid 2,\Delta t) & P(1\mid 3,\Delta t) \\ P(2\mid 0,\Delta t) & P(2\mid 1,\Delta t) & P(2\mid 2,\Delta t) & P(2\mid 3,\Delta t) \\ P(3\mid 0,\Delta t) & P(3\mid 1,\Delta t) & P(3\mid 2,\Delta t) & P(3\mid 3,\Delta t) \end{pmatrix} =$$

$$\begin{pmatrix} 1-3\alpha_h\Delta t & 3\alpha_h\Delta t & 0 & 0 \\ \beta_h\Delta t & 1-(\beta_h+2\alpha_h)\Delta t & 2\alpha_h\Delta t & 0 \\ 0 & 2\beta_h\Delta t & 1-(\alpha_h+2\beta_h)\Delta t & \alpha_h\Delta t \\ 0 & 0 & 3\beta_h\Delta t & 1-3\beta_h \end{pmatrix} \qquad (13)$$

A simple way to implement the stochastic scheme for N channels is to simulate each channel with the transition probability matrix given by (13) and then count the number of channels in the open-state S_3. If we are mostly interested in a small cluster, such a procedure is sufficiently efficient and easy to implement.

A more efficient scheme can be put together by grouping the IP_3Rs into sets of channels with n open h-gates, where n=0,1,2,3. If there are N_n IP_3Rs in state S_n and the channels are all independent, the probabilities that m IP_3Rs switch into the states S_{n+1} or S_{n-1} (by opening or closing an h-gate) within Δt are given by the binomial distributions (see e.g. (Schneidman et al. 1998))

$$\begin{aligned} P_{n\to n+1}(m,\Delta t) &= \binom{N_n}{m} P(n\mid n+1,\Delta t)^m \left(1-P(n\mid n+1,\Delta t)\right)^{N_n-m} \\ P_{n\to n-1}(m,\Delta t) &= \binom{N_n}{m} P(n\mid n-1,\Delta t)^m \left(1-P(n\mid n-1,\Delta t)\right)^{N_n-m} \end{aligned}, \qquad (14)$$

with transition probabilities in (13). There are numerous schemes how to update the occupation numbers N_n during one time step. We start with the fastest process (largest transition probability) and then move to the next slower one and so on. We now discuss concrete results obtained with the stochastic Li-Rinzel model.

12.2.3 Calcium release by an isolated cluster of IP_3Rs

We consider a cluster of N IP_3Rs that are spatially close enough so that it can be assumed that the calcium concentration is uniform across the cluster. Given a cluster diameter of about 100nm, the diffusion time

$$\tau_D = \frac{L^2}{D} \approx \frac{(100nm)^2}{50\left(\mu m^2/s\right)} = 200\mu s \qquad (15)$$

which is more than three orders of magnitude smaller than the time scale of the Li-Rinzel model (seconds). Trajectories obtained from a cluster of 20 IP_3Rs are shown for three different values of p=[IP_3] in Fig.5. For [IP_3]=0.3μM, i.e. below the Hopf-bifurcation of the deterministic model ([IP_3]=0.345μM), a trace is shown in Fig.5a. While the deterministic equation predicts a fix point (see Fig.3), the stochastic dynamics generates release events where a significant fraction of the

IP_3Rs open up for a short amount of time to release a puff of calcium into the intracellular space. The trajectory for $[IP_3]=0.5\mu M$ is shown in Fig.5b. While the deterministic solution (see Fig.3) predicts periodic calcium oscillations, the stochastic model generates a spike train that looks not very different from the trajectory for sub-threshold $[IP_3]$. The situation is similar for $[IP_3]=0.8\mu M$ in Fig.5c.

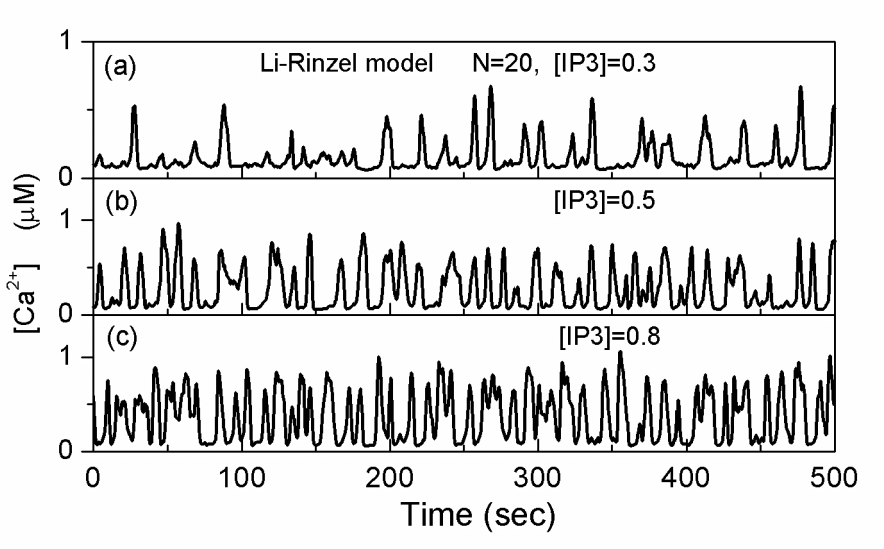

Fig. 5. Calcium traces obtained from the stochastic Li-Rinzel for a cluster of 20 IP_3Rs at three characteristic values of $[IP_3]$. The time (horizontal axis) is measured in seonds.

The most important conclusion from this observation is that a cluster of as few as 20 IP_3Rs, a size which is believed to be realistic, cannot be described by a set of kinetic equations such as the deterministic DeYoung-Keizer model or the Li-Rinzel model. Stochastic methods are necessary.

12.2.4. Langevin Approximation to the Stochastic Li-Rinzel Model

The drawback of the stochastic methods described here is that they become computationally very demanding as one wishes to describe an entire cell with thousands of release clusters or even networks of cells. In the following we describe an alternative scheme resulting in stochastic differential equations (Langevin equations) that are easy to implement and computationally very efficient. The first approximation is that all three *h*-subunits can be replaced by a single two-state subunit with the same opening and closing rates $\alpha(p)$ and $\beta(c)$.

This assumption can be somewhat motivated but justified only by the success of the resulting Langevin equations. The motivation is that all subunits are clamped to the same Ca^{2+} concentration and their opening and closing events are thus somewhat correlated. For a fixed Ca^{2+} concentration, the probability of finding N open single-subunit channels in a cluster of N_t channels obeys the birth-death master equation

$$\frac{\partial P(N,t)}{\partial t} = G^+(N-1)P(N-1,t) - \left(G^+(N)+G^-(N)\right)P(N,t) + G^-(N+1)P(N+1,t) \tag{16}$$

where

$$\begin{aligned} G^+(N) &= (N_t - N)\alpha_h \\ G^-(N) &= N\beta_h \end{aligned} \quad . \tag{17}$$

The following scaling transformation

$$\begin{aligned} n &= N / N_t \\ g^+(n) &\equiv \frac{G^+(N)}{N_t} = (1-n)\alpha_h \\ g^-(n) &\equiv \frac{G^-(N)}{N_t} = n\beta_h \\ \rho(n) &\equiv P(N_t n) \end{aligned} \quad , \tag{18}$$

and the subsequent Taylor-expansion in powers of $\varepsilon = 1/N_t$

$$\begin{aligned} G^+(N-1) &= G^+\left(N_t(n-\varepsilon)\right) = g^+(n-\varepsilon) = g^+(n) + \sum_{i=1}^{\infty}\frac{1}{i!}\varepsilon^i\left(-\frac{\partial}{\partial n}\right)^i g^+(n) \\ G^-(N+1) &= G^-\left(N_t(n+\varepsilon)\right) = g^-(n+\varepsilon) = g^-(n) + \sum_{i=1}^{\infty}\frac{1}{i!}\varepsilon^i\left(\frac{\partial}{\partial n}\right)^i g^-(n) \\ P(N+1) &= P\left(N_t(n+\varepsilon)\right) = \rho(n+\varepsilon) = \rho(n) + \sum_{i=1}^{\infty}\frac{1}{i!}\varepsilon^i\left(\frac{\partial}{\partial n}\right)^i \rho(n) \\ P(N-1) &= P\left(N_t(n-\varepsilon)\right) = \rho(n-\varepsilon) = \rho(n) + \sum_{i=1}^{\infty}\frac{1}{i!}\varepsilon^i\left(-\frac{\partial}{\partial n}\right)^i \rho(n) \end{aligned} \quad , \tag{19}$$

yields after inserting (19) into (16) and comparing coefficients of equal powers in ε the Kramers-Moyal expansion

$$\frac{\partial \rho(n,t)}{\partial t} = \sum_{i=1}^{\infty} \frac{1}{i!} \varepsilon^{i-1} \left(-\frac{\partial}{\partial n} \right)^i M_i(n) \rho(n,t) \quad , \tag{20}$$

with the Kramers–Moyal coefficients

$$M_i(n) = g^+(n) + (-1)^i g^-(n) = (1-n)\alpha_h + (-1)^i n\beta_h \quad . \tag{21}$$

We truncate the Kramers-Moyal expansion after the second term (the diffusion term) and obtain the Fokker-Planck equation

$$\frac{\partial \rho(n,t)}{\partial t} = -\frac{\partial}{\partial n} M_1(n)\rho(n,t) + \frac{1}{2N_t} \frac{\partial^2}{\partial n^2} M_2(n)\rho(n,t) \quad , \tag{22}$$

with the drift and diffusion coefficients

$$\begin{aligned} M_1(n) &= g^+(n) - g^-(n) = (1-n)\alpha_h - n\beta_h \\ M_2(n) &= g^+(n) + g^-(n) = (1-n)\alpha_h + n\beta_h \end{aligned} \quad . \tag{23}$$

Note that this truncation does not guarantee the preservation of the exact stationary probability (Hänggi and Jung 1988). An equivalent Ito-type Langevin equation can be found as

$$\begin{aligned} &\frac{dn}{dt} = \alpha_h(1-n) - \beta_h n + \xi(t) \\ &\langle \xi(t)\xi(t') \rangle = \frac{\alpha_h(1-n) + \beta_h n}{N_t} \delta(t-t') \\ &\langle \xi(t) \rangle = 0 \end{aligned} \quad , \tag{24}$$

with Gaussian, white noise ξ(t). Fox and Lu (1994) and later Schmid et al. (2001) have used such a scheme to describe action potentials generated by clusters of neuronal ion channels. The Langevin approximation of the stochastic Li-Rinzel model thus reads

$$\begin{aligned} &\frac{dc}{dt} = -c_1 m_\infty^3 n_\infty^3 h^3 (c - c_{ER}) - c_1 v_2 (c - c_{ER}) - \frac{v_3 c^2}{k_3^2 + c^2} \\ &\frac{dh}{dt} = \alpha_h(1-h) - \beta_h h + \xi(t) \\ &\langle \xi(t)\xi(t') \rangle = \frac{\alpha_h(1-h) + \beta_h h}{N_t} \delta(t-t') \\ &\langle \xi(t) \rangle = 0 \end{aligned} \quad . \tag{25}$$

It is almost as simple as the deterministic Li-Rinzel model except for the noise term in the second equation.

Integrating these equations with a first order solver, the stochastic term results in one additional term

$$h(t+\Delta t) = \left(\alpha_h (1-h(t)) - \beta_h h(t)\right)\Delta t + \sqrt{2K\Delta t}\, R_t \qquad (26)$$

$$K = \frac{\alpha_h (1-n) + \beta_h n}{N_t} \quad ,$$

where R_t denotes a Gaussian random number with unit variance. The most significant advantages of the Langevin equations are that they are simple to implement and that their computational demand does not grow with increasing cluster size N_t.

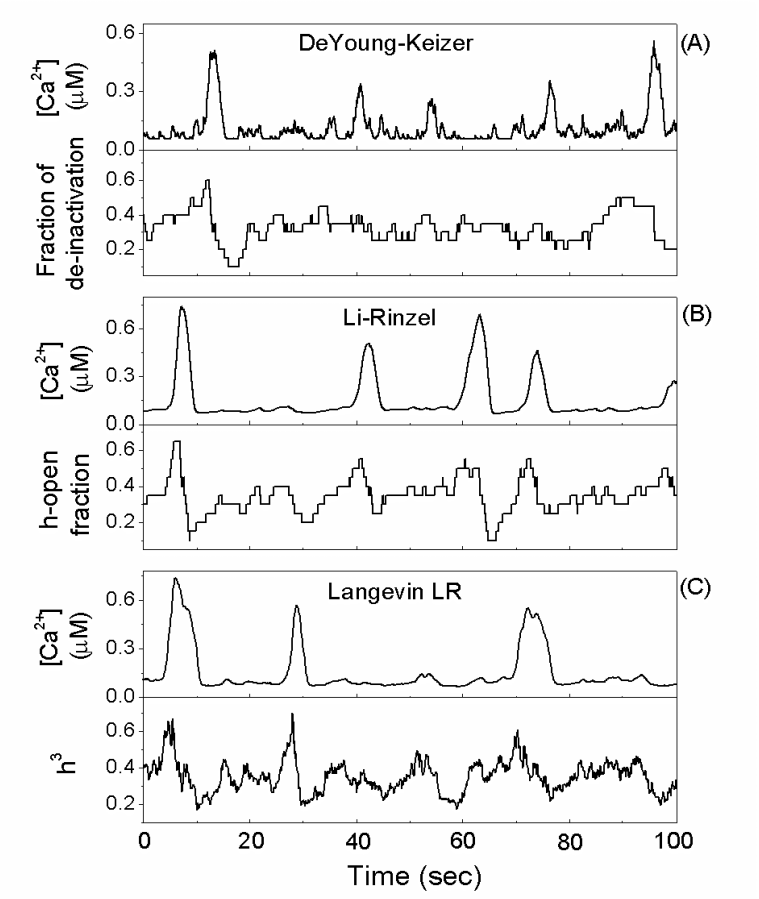

Fig. 6. Simulation results obtained from three models (DeYoung-Keizer (A), Li-Rinzel (B), Langevin (C)) of an isolated cluster of 20 IP_3Rs.

12.3. Results

12.3.1 Calcium Release Dynamics

In this section we compare the time traces of calcium released by isolated, mostly small, clusters of IP_3Rs, obtained from the models described above. In Fig.6, the upper panel (A) shows the intracellular Ca^{2+} concentration obtained with the DeYoung-Keizer model for a time interval of 100s. Below, we show the fraction of channels that are de-inhibited to compare with the corresponding fractions obtained with the other methods. Panel (B) shows a Ca^{2+} trace and the corresponding fraction of *h*-open channels during 100s of simulation obtained with the stochastic Li-Rinzel model. Panel (C) shows the corresponding data obtained with the Langevin approach. The Ca^{2+} trace obtained from the DeYoung-Keizer model has more high-frequency content since the Li-Rinzel and Langevin approach are obtained from the DeYoung-Keizer model after eliminating fast time scales. In all three cases, large fractions of de-inhibited channels correlate with peaks in the calcium release (puffs). For the Langevin approach, the inactivation variable *h* is continuous while it is discrete for the Markov-approaches.

We made more detailed comparisons of the statistical moments of the stochastic Ca^{2+} traces at different cluster sizes and concentrations of IP_3 (Fig.7). The stochastic Li-Rinzel model reproduces the data of the DeYoung-Keizer model remarkably well for cluster sizes larger than 10 channels. More surprising, although the Langevin approach is derived for large cluster sizes, it works very well for clusters larger than 100 channels and reasonably well even for clusters of 20 channels. At 20 channels, the mean value obtained from the Langevin equation is about 7% off the mean value obtained from the DeYoung-Keizer Model. In Fig.8, we compare the mean values and the variances of the Ca^{2+} signal generated by a cluster of 20 IP_3Rs as a function of $[IP_3]$.

The agreement is good throughout. Also the fractions of de-inhibited channels, important for the stochastic Li-Rinzel and the Langevin models, are in good agreement between the models. This is demonstrated in Fig.9, where we compare the fraction of de-inactiavted channels obtained from the DeYoung-Keizer model with the fraction of *h*-open channels of the stochastic Li-Rinzel model and the continuous *h*-open fraction of the Langevin approach for three different of IP_3 concentration.

12.3.2. Puff Amplitude Distributions

Another measure used in experiments to characterize calcium puffs is the puff-amplitude distribution. During each calcium puff, the maximum Ca^{2+} concentration is recorded (Pratusevich and Balke 1996, Bootman et al. 1997; Smith et al. 1998, Izu et al. 1998, Sun et al. 1998, Thomas et al. 1998, Cheng et al.

1999, Jiang et al. 1999, Callamaras and Parker 2000, Marchant and Parker 2001, Rios et al. 2001). We have computed histograms of these puff-amplitudes using the three stochastic methods.

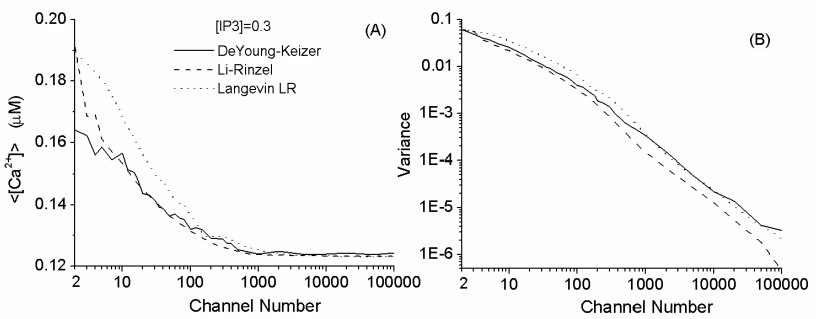

Fig. 7. In panel (A) the mean cytosolic Ca^{2+} concentrations are shown as a function of the number of IP_3Rs per cluster at a fixed sub-threshold concentration of [IP3]=0.3μM for all three different schemes. In panel (B), the variances of the stochastic Ca^{2+} concentration are shown.

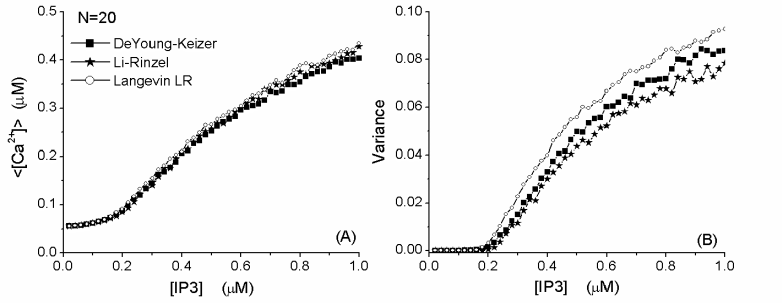

Fig. 8. The mean values (A) and the variances (B) generated by a cluster of 20 IP_3Rs are compared for different concentrations of $[IP_3]$. The three models are compared. Note the different scale in conparison to Fig.7.

It is clear from Fig.6, that the DeYoung-Keizer model generates more small puffs than the other methods since for the other methods, the fast time scales have been eliminated. From the upper panel of Fig.6 it also clear that these fast puffs are smaller puffs. The question therefore is whether the larger and slower puffs produced by the Li-Rinzel and the Langevin model match those of the DeYoung-Keizer model. In order to compare these, we filter the Ca^{2+} time series by eliminating puffs below a cut-off size. The remaining puffs are analyzed with respect to their amplitudes and re-normalized to one. In Figs.10A,B we compare the puff-amplitude distributions of the filtered puffs from the DeYoung-Keizer model with the puff amplitude distributions obtained from the stochastic Li-Rinzel

and the Langevin models at [IP_3]=0.3μM (Fig.10A) and [IP_3]=0.5μM (Fig.10B), using two different cut-off sizes, 0.2μM(upper panels A) and 0.4μM (lower panels B). The distributions are in qualitative agreement at the higher cut- off threshold of 0.4μM.

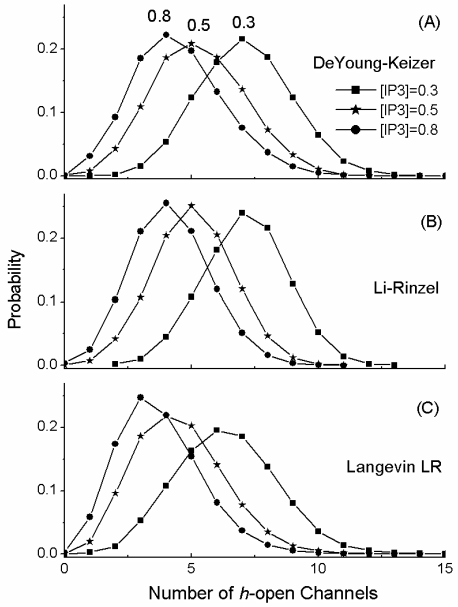

Fig. 9. Distribution of open de-inhibited channels of the DeYoung-Keizer model (A) compared with the distribution of *h*-open channels obtained from the stochastic Li-Rinzel model (B) and the Langevin model (C) for three charecteristic values of [IP_3]. The data were obtained from a cluster with 20 IP_3Rs.

Depending on the concentration of IP_3 and the number of channels for the cluster, the puff amplitude distribution can assume quite different shapes. Generally for small concentrations of IP_3, the puff-amplitude distribution is monotonously decaying. When the concentration approaches the critical value at which oscillations set in (first Hopf bifurcation, see Fig.6) in the deterministic system, the puff - amplitude distributions develop additional peaks, indicating characteristic amplitudes. When [IP_3] exceeds the concentration at which the other Hopf bifurcation occurs, a single peak remains at a larger Ca^{2+} concentration. A more detailed sketch of the shapes of the puff-amplitude distributions under various conditions is shown in Fig.11.

12.3.3. Puff-width Distributions

Another quantity that is often measured in the context of calcium puffs is the distribution of the temporal width of a puff released from a single release cluster (Sun et al. 1998, Thomas et al. 1998; Haak et al. 2001). We define the width as the time interval during which the Ca^{2+} amplitude exceeds half its peak value. To compare puff-width distributions obtained from the stochastic DeYoung-Keizer model in a meaningful way with those obtained with the other methods, the same filtering as described in Sect. 3.2 has been applied. The results are shown in Fig.12. It is quite remarkable how the enhanced filtering (B) results in good agreement for all three methods.

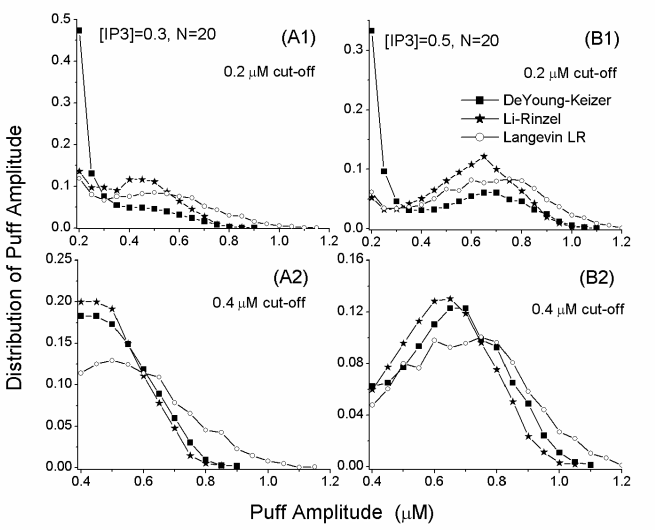

Fig. 10. Puff amplitude distributions of a cluster with 20 IP_3Rs at $[IP_3]$=0.3μM (A) and 0.5μM (B). In the upper panels (A1,B1) we have used a cut-off size of 0.2μM while 0.4μM has been used in the lower panels (A2,B2)

12.3.4. Inter-puff Interval Distributions

Another quantity characterizing Ca^{2+} puffs is the distribution of the time intervals between two consecutive puffs (Marchant et al 1999). To compare inter-puff interval distributions obtained from the stochastic DeYoung-Keizer model in a meaningful way with those obtained with the other methods, the same filtering as described in Sect. 3.2 has been applied. The results are shown in Fig.13. While for a low cut-off value for puffs (panels A1,B1), the DeYoung-Keizer model exhibits an inter-puff interval distribution with more short intervals, additional size

filtering with a threshold twice as large (A2,B2) yields good agreement between the inter-puff interval distributions obtained with all three methods.

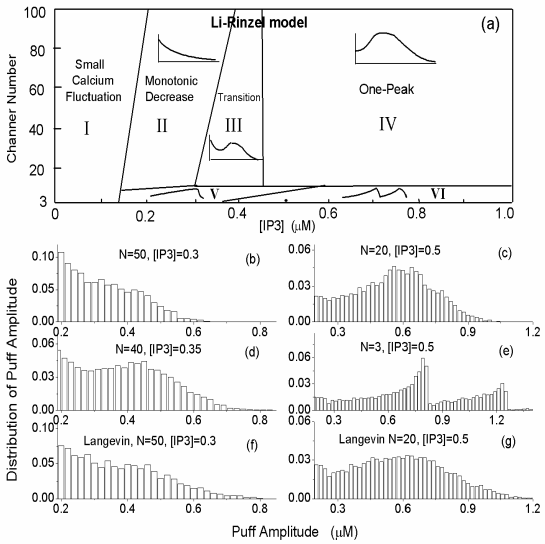

Fig. 11. The *phase diagram* of the puff amplitude distributions is shown in (a) in the [IP_3]–N plane. Samples of puff amplitude distributions obtained with the stochastic Li-Rinzel model are shown in b-e in various regimes indicated in (a). Figures f and g show the amplitude distribution obtained with the Langevin method in comparison to those obtained with the full kinetic method in b and c.

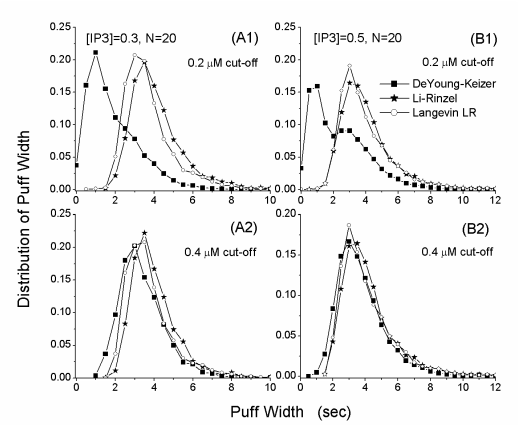

Fig. 12. The puff-width distributions generated from a cluster of 20 IP_3Rs using the three stochastic methods are compared for two different values of [IP_3] and for different cut-off values. The cut-off value in the upper panels (A1,B1) is 0.2μM and in the lower panels (A2,B2) 0.4μM.

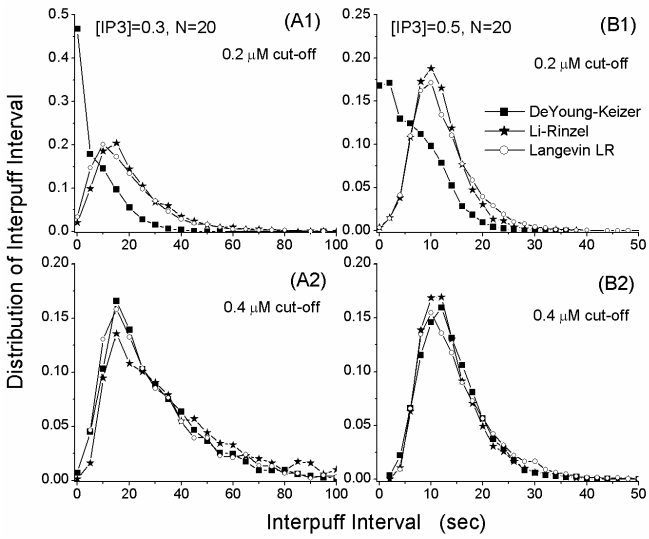

Fig. 13. Distributions of inter-puff intervals generated from a cluster of 20 IP_3Rs using the three stochastic methods are compared for two different values of $[IP_3]$ and for different cut-off values. The cut-off value in the upper panels (A1,B1) is 0.2μM and in the lower panels (A2,B2) 0.4μM.

12.3.5. Large Clusters – The deterministic Limit

In this section, we show that for large channel numbers, the stochastic schemes approach the appropriate deterministic limits. In case of the Langevin approach this is quite obvious since the noise-term in the second equation of (26) vanishes in the limit of large N_t. For the other models, the deterministic limit given by the DeYoung-Keizer model and the Li-Rinzel model will also be approached since the master equations for the multiple subunits can be expanded in completely analogous ways. In Fig.14, we compare the bifurcation diagram for the stochastic Li-Rinzel model and the stochastic DeYoung-Keizer model for a cluster of 10,000 channels with the respective deterministic limits. The minima and the maxima of the stochastic Ca^{2+} traces have been obtained by averaging over local minima and maxima, respectively. While the expectation values agree already very well with the deterministic limits, there are still substantial deviations from the deterministic limit in the bifurcation diagram for large concentrations of IP_3. For larger clusters these differences vanish (not shown here).

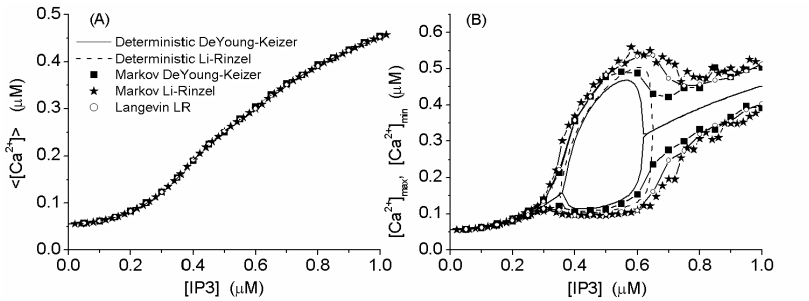

Fig. 14. The average calcium concentration obtained with all three stochastic methods from a cluster of 10,000 IP_3Rs (A). The bifurcation diagrams obtained with all three stochastic methods in comparison with their respective deterministic limits (see also Fig.5) for a cluster of 10,000 IP_3Rs (B).

12.4. Conclusions

Stochastic modeling of IP_3Rs using Markov-methods is computationally very demanding. For whole-cell modeling or even intercellular modeling of Ca^{2+} signaling, computational efficiency becomes an important factor. To meet the need for a fast algorithm, we have put forward a Langevin equation to describe the release of Ca^{2+} by an isolated cluster of IP_3Rs. Although the Langevin equation is derived for large numbers of channels it turns out to produce results that are in good agreement with the DeYoung-Keizer model even for clusters as small as 20 channels. We have compared bifurcation diagrams, puff amplitude distributions, puff-width distributions and inter-puff interval distributions.

This material is based on work supported by National Science Foundation under grant IBN 0078055

References

Bezprovanny I, Watras J, Ehrlich B (1991) Bell-shaped calcium response curves of $Ins(1,4,5)P_3$- and calcium-gated channels from endoplasmic reticulum of cerebellum. Nature. 351: 751-754.

Bootman, M, Niggli E, Berridge M, Lipp P (1997) Imaging the hierarchical Ca^{2+} signaling system in HeLa cells. The Journal of Physiology 499: 307-314.

Callamaras NJ, Marchant S, Sun X, Parker I (1998) Activation and co-ordination of $InsP_3$ mediated elementary Ca^{2+} events during global Ca^{2+} signals in Xenopus oocytes, Journal of Physiology 509: 81-91.

Callamaras N, Parker I (2000) Phasic characteristic of elementary Ca^{2+} release sites underlies quantal responses to IP_3. The EMBO Journal 19: 3608-3617.

Cheng HW, Lederer J, Cannel MB (1993) Calcium sparks elementary events underlying excitation-contraction coupling in heart muscle. Science 262: 740-744.

Cheng H, Song L, Shirokova N, Gonzalez A, Lakatta EG, Rios E, Stern MD (1999) Amplitude distribution of calcium sparks in confocal images: theory and studies with an automatic detection method. Biophys. J. 76: 606-617.

DeYoung GW, Keizer J (1992) A single-pool inositol 1,4,5-trisphosphate-receptor-based model for agonist-stimulated oscillations in Ca^{2+} concentration. Proceedings of the National Academy of Sciences USA, 89: 9895 - 9899.

Fox RF, Lu Y (1994). Emergent collective behavior in large numbers of globally coupled independently stochastic ion channels. Phys. Rev. E. 62: 2636-2643.

Gonzalez A, Kirsch WG, Shirokova N, Pizarro G, Brum G, Pessah IN, Stern MD, Cheng H, and Rios E (2000) Involvement of multiple intracellular release channels in calcium sparks of skeletal muscle. Proceeding of the National Academy of Sciences USA 97: 4380-4385.

Haak, LL, Song L, Molinski TF, Pessah IN, Cheng H, Russell JT (2001) Sparks and puffs in oligodendrocyte progenitors: cross talk between Ryanodine receptors and inositol trisphosphate receptors. Journal of Neuroscience. 21: 3860-3870.

Hänggi P, Jung P (1988) Bistability in Active Circuits: Application of a novel Fokker-Planck Approach. IBM Jorunal of Research and Development 32:119-125

Izu LG, Wier WG, Balke CW (1998) Theoretical analysis of the Ca^{2+} spark amplitude distribution. Biophysical Journal, 75: 1144-1162.

Jiang Y, Klein MG, Schneider MF. 1999. Numerical simulation of Ca^{2+} sparks in skeletal muscle. Biophys. J. 77: 2333-2357.

Keener J and Sneyd J (2000) Mathematical Physiology. Springer, New York

Li Y, Rinzel J (1994). Equations for IP_3 receptor-mediated Ca^{2+} oscillations derived from a detailed kinetic model: a Hodgkin-Huxley like formalism. Journal of Theoretical Biology 166:461-473.

Lipp P. Niggli E (1998) Fundamental calcium release events revealed by two-photon excitation photolysis of caged calcium in guinea-pig cardiac myocytes. Journal of Physiology 508: 801-809.

Marchant J, Callamaras N, Parker I (1999) Initiation of IP_3 mediated Ca^{2+} waves in Xenopus oocytes. The EMBO Journal 19: 5285-5299.

Marchant JS, Parker I (2001) Role of elementary Ca^{2+} puffs in generating repetitive Ca^{2+} oscillations. The EMBO Journal 20: 65-76.

Mak, DD, Foskett JK (1997) Single-channel kinetics inactivation, and spatial distribution of Inositol Trisphosphate receptors in Xenopus oocyte nucleus. Journal of General Physiology 109: 571-587.

Melamed-Book N, Kachalsky SG, Kaiserman I, Rahamimoff R (1999) Neuronal calcium sparks and intracellular calcium noise. Proceeding of the National Academy of Sciences USA. 26: 15217 - 15221.

Pratusevich VR, Balke CW (1996) Factors shaping the confocal image of the calcium spark in cardiac muscle cells. Biophys. J. 71: 2942-2957.

Rios EN, Shirokova W, Kirsch G, Pizarro MD, Stern H, Cheng H, Gonzalez A (2001) A preferred amplitude of calcium sparks in skeletal muscle. Biophys. J. 80: 169-183.

Schmid G, Goychuk I, P. Hanggi P (2001) Stochastic resonance as a collective property of ion channel assemblies. Europhys. Lett. 56: 22-30

Schneidman E., Freedman B., and Segev I. (1998) Ion channel stochasticity may be critical in determining the reliability and precision of spike timing. Neural Computation 10:1679 - 1703

Smith GD, Keizer JE, Stern MD, Lederer WJ, Cheng H (1998) A simple numerical model of calcium spark formation and detection in cardiac myocytes. Biophys. J. 75: 15-32.

Sun XN, Callamaras NJ, Marchant JS, Parker I (1998) A continuum of $InsP^3$-mediated elementary Ca^{2+} signaling events in Xenopus oocytes. Journal of Physiology 509: 67-80.

Thomas D, Lipp P, Berridge MJ, Bootman MD (1998) Hormone-evoked elementary Ca^{2+} signals are not stereotypic, but reflect activation of different size channel clusters and variable recruitment of channels within a cluster. The Journal of Biological Chemistry 273: 27130-27136.